RESEARCH PAPER

Wafer-scale fabrication of uniform Si nanowire arrays using the Si wafer with UV/Ozone pretreatment

**Fan Bai · Meicheng Li · Rui Huang · Yue Yu ·
Tiansheng Gu · Zhao Chen · Huiyang Fan ·
Bing Jiang**

Abstract The electroless etching technique combined with the process of UV/Ozone pretreatment is presented for wafer-scale fabrication of the silicon nanowire (SiNW) arrays. The high-level uniformity of the SiNW arrays is estimated by the value below 0.2 of the relative standard deviation of the reflection spectra on the 4-in. wafer. Influence of the UV/Ozone pretreatment on the formation of SiNW arrays is investigated. It is seen that a very thin SiO_2 produced by the UV/Ozone pretreatment improves the uniform nucleation of Ag nanoparticles (NPs) on the Si surface because of the effective surface passivation. Meanwhile, the SiO_2 located among the adjacent Ag NPs can obstruct the assimilation growth of Ag NPs, facilitating the deposition of the uniform and dense Ag NPs catalysts, which induces the formation of the SiNW arrays with good uniformity and high filling ratio. Furthermore, the remarkable antireflective and hydrophobic properties are observed for the SiNW arrays which display great potential in self-cleaning antireflection applications.

Introduction

Silicon nanowire (SiNW) arrays have attracted great research interest in the recent years because of their potential applications in various fields of energy conversion and storage (Jung et al. 2013; Chan et al. 2008), photocatalysis (Wang et al. 2012a, b), chemical and biological sensors (Mcalpine et al. 2007; Peng et al. 2009), etc. In particular, SiNW arrays have been employed in Si-based solar cells as a self-cleaning antireflective layer because of their remarkable hydrophobic and antireflective properties (He et al. 2011; Dai et al. 2010; Geng et al. 2012). To bring the SiNW arrays to the market on a commercial scale, one of the remaining challenges is the wafer-scale production of the uniform SiNW arrays.

A few methods have been developed to fabricate SiNW arrays to date. The commonly used bottom-up approaches (i.e., typical vapor–liquid–solid growth (Krylyuk et al. 2011)) are difficult to realize the

F. Bai · M. Li
School of Materials Science and Engineering, Harbin
Institute of Technology, Harbin 150001, China

F. Bai · M. Li (✉) · R. Huang · Y. Yu ·
T. Gu · Z. Chen · H. Fan · B. Jiang
State Key Laboratory of Alternate Electrical Power
System with Renewable Energy Sources, School of
Renewable Energy, North China Electric Power
University, Beijing 102206, China
e-mail: mcli@ncepu.edu.cn

M. Li
Suzhou Institute, North China Electric Power University,
Suzhou 215123, China

wafer-scale fabrication of SiNW arrays because the growth rate of SiNW arrays greatly varies along the blow gas direction on the whole wafer (Tamboli et al. 2012). Dry etching provides a feasible route for producing wafer-scale SiNW arrays (Morton et al. 2008). Unfortunately, these vacuum-based approaches usually require expensive equipments, which increase fabrication cost. At the same time, a metal-assisted electroless etching (MAEE) method has been proposed for low-cost fabrication of SiNW arrays (Wang et al. 2012a, b; Peng et al. 2007; Shiu et al. 2011). In the MAEE process, to achieve the wafer-scale SiNW arrays, uniform deposition of metal nanoparticle (NPs)-based catalysts on Si wafer is crucial. A few templates, such as porous anodic alumina (Wang et al. 2012a, b) and polystyrene spheres (Peng et al. 2007), are usually employed to improve uniformity of metal NPs on Si wafer. However, these masking processes introduce complexity which limits their practical application. Recently, it has been found that the surface states of Si affect the size, density, and coverage of the metal NPs during the electroless plating process (Shiu et al. 2011; Yae et al. 2007). As we know, the surface states can be modified by the pretreatment. Therefore, surface pretreatment technique provides the possibility for achieving the uniform deposition of metal NPs on Si wafer, which enables the facile and cost-efficient fabrication of wafer-scale uniform SiNW arrays.

In this study, we develop an electroless etching technique combined with the process of UV/Ozone pretreatment to produce SiNW arrays on 4-in. wafer. High-level uniformity of SiNW arrays in the wafer-scale has been obtained. Furthermore, the mechanism of UV/Ozone pretreatment with respect to the uniform formation of the wafer-scale SiNW arrays is investigated. Moreover, the uniform SiNW arrays with antireflective and hydrophobic characteristics display great potential in self-cleaning antireflection applications.

Experimental

Single crystalline n-type Si(100) wafers (with the resistivity of 3–5 Ω cm) are used for the experiment. All Si samples are cleaned using acetone, absolute ethyl alcohol, and deionized water in the ultrasonic condition, respectively. The Si samples are then polished using a CP-4A solution mixed with HF, HNO_3, CH_3COOH, and H_2O in a volume ratio of 3:5:3:22. The polished Si samples are immediately dipped into a 7.3 M HF solution forming the H-terminated surfaces, which are subsequently exposed in a UV/Ozone environment. The SiNW arrays are fabricated by a MAEE method (Bai et al. 2012).

Surface chemistry of the pretreated Si samples is analyzed using an X-ray photoelectron spectrometer with a Thermo Fisher K-Alpha. Surface morphologies of the Ag NPs and the SiNW arrays are observed using a scanning electron microscope (SEM) with a FEI Quanta 200F. The reflection spectra of the SiNW arrays are detected using a solar cell IPCE/QE measurement system with an integrating sphere. The contact angles of the SiNW arrays are measured via the sessile drop method using 10-µL DI water droplets at room temperature.

Results and discussion

Figure 1 shows the photograph of the 4-in. wafer covered with SiNW arrays, which are obtained using the electroless etching technique with our UV/Ozone pretreatment process. Compared with the original wafer, the 4-in. wafer appears equally black in color, as shown in Fig. 1, suggesting that SiNW arrays cover over the entire 4-in. wafer uniformly. Meanwhile, the morphology of SiNW arrays is characterized at four random areas by SEM technique. For any other areas on the wafer, the SiNW arrays all appear with the similar morphology, filling ratio (of about 1.1×10^{10} cm^{-2}), and length (of about 3.2 µm), as shown in Fig. 1a–d.

To further evaluate the wafer-scale uniformity of SiNW arrays, the reflection spectra of SiNW arrays at selected 30 areas on the 4-in. wafer are detected, and the corresponding spectral data are shown as the curves (a) in Fig. 2. Here, the different areas on the wafer are positioned following the dots with a periodic gap of 1.3 cm (inset in Fig. 2). As we know, the reflection spectra of SiNW arrays are sensitive to their structural parameters, including the length, diameter, and filling ratio. In view of this aspect, the structural differences at different dots can be qualitatively
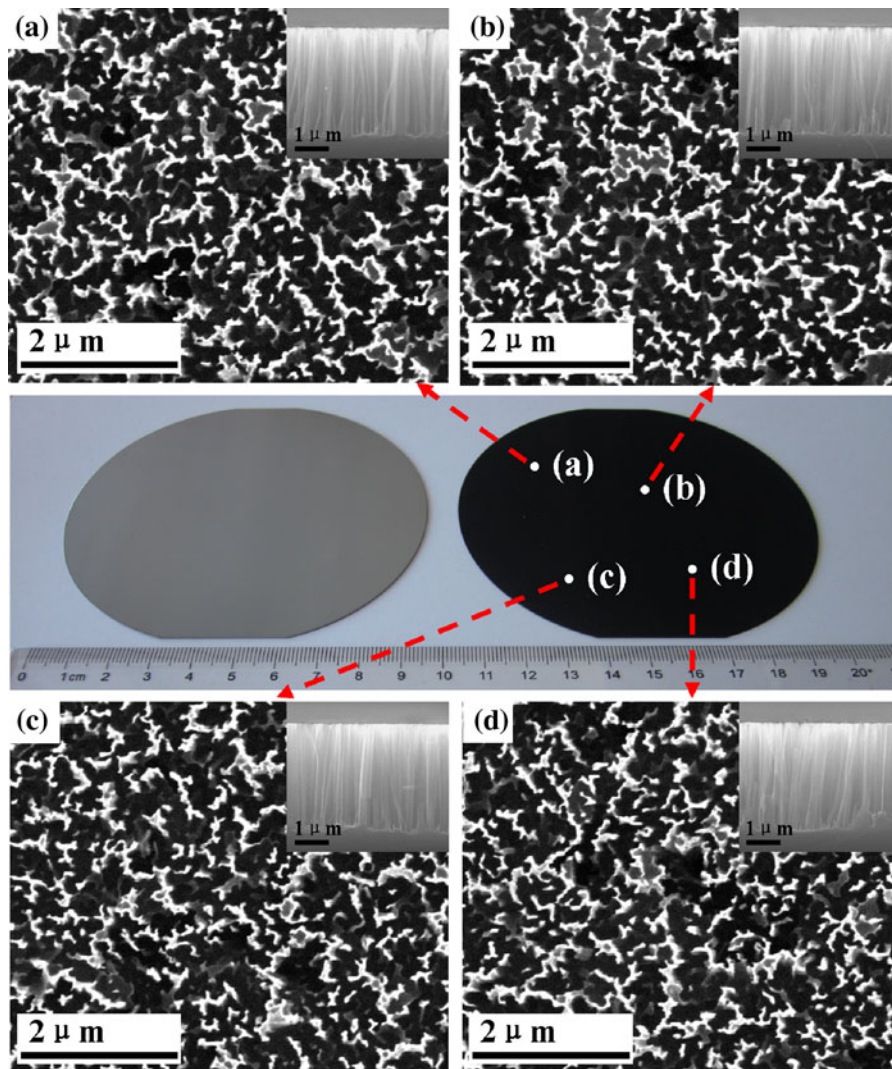
Fig. 1 Pictures of 4-in. SiNW arrays obtained by etching Si wafer with UV/Ozone pretreatment in HF/AgNO$_3$ solution for 20 min; **a–d** are planar-viewed and cross-sectional SEM images of random areas on a 4-in. wafer covered with SiNW arrays as shown on the surface of the *black wafer*

evaluated by their reflection spectral variations. To clearly observe the reflection spectral variations of SiNW arrays at different dots, the relative standard deviations (RSDs) of the corresponding spectral data are calculated. These data are written as matrices W and R. Matrix W represents an array of w_m representing different wavelength values, and matrix R the arrays of $r_{m,n}$, that is the reflectance values corresponding to the different wavelengths at some dot of the 4-in. wafer. The RSDs of the values in each row of matrix R are calculated, and the results are recorded as the matrix D.

$$W = \begin{bmatrix} w_1 \\ w_2 \\ \cdots \\ w_m \end{bmatrix}, \quad R = \begin{bmatrix} r_{1,1} & r_{1,2} & \cdots & r_{1,30} \\ r_{2,1} & r_{2,2} & \cdots & r_{2,30} \\ \cdots & \cdots & \cdots & \cdots \\ r_{m,1} & r_{m,2} & \cdots & r_{m,30} \end{bmatrix},$$

$$D = \begin{bmatrix} d_1 \\ d_2 \\ \cdots \\ d_m \end{bmatrix}$$

According to the matrix W and matrix D, the RSD curve as a function of the wavelength is plotted as the
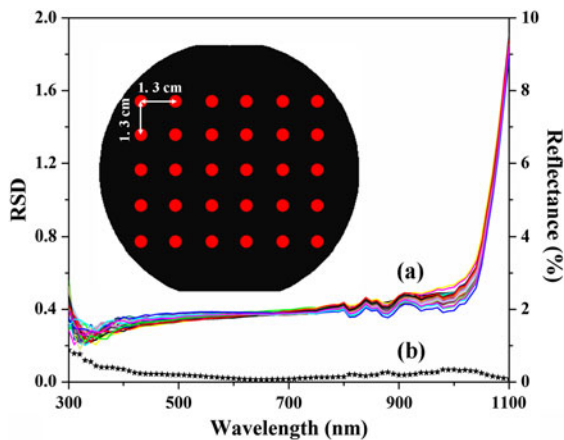
Fig. 2 (*a*) Reflection spectra of the 4-in. SiNW arrays collected on 30 *dots*. (*b*) The *curves* of the corresponding RSD values; *Inset* shows the diagram of 30 *dots* with a periodic distance of 1.3 cm on the wafer

curve (b) in Fig. 2. The RSD values in the wavelength ranges of 300–1,100 nm are all less than 0.2, suggesting that the SiNW arrays are wafer-scale uniform. These results indicate that the formation of wafer-scale uniform SiNW arrays has been realized using the UV/Ozone-pretreated Si wafer.

To understand the role of UV/Ozone-pretreated surface on the formation of SiNW arrays, surface chemistry of the Si samples with conventional HF pretreatment and the UV/Ozone pretreatment are analyzed, respectively. The HF processing yields one O 1s binding energy at 531.6 eV (Fig. 3a), implying that the hydroxyl groups are present as the silanol (Si–OH) beside the H-terminated bonds (Zazzera and Moulder 1989). After the pretreatment with UV/Ozone, binding energy of the O 1 s shifts from 531.6 to 532.2 eV while its intensity has a threefold increase, indicating that the oxide is introduced into the Si surface after UV/Ozone pretreatment. The Si 2p photoelectron spectra (Fig. 3b) show that the UV/Ozone pretreatment produces a chemical shift of 4 eV, indicating that the oxide is present as SiO_2. The thickness of SiO_2 layer is estimated at 0.8 nm according to the previous report (Zazzera and Moulder 1989). These results suggest that the UV/Ozone-pretreated process yields a very thin SiO_2 layer on the Si surfaces.

The morphology of SiNW arrays is closely associated to that of the Ag NPs catalysts. To examine the effect of UV/Ozone pretreatment on the formation of

SiNW arrays, the Si wafer with the UV/Ozone-pretreated surface is immersed in $HF/AgNO_3$ solution for 5 s to observe the morphology of the in situ Ag NPs as shown in Fig. 4a. It can be seen that the isolated island-like Ag NPs form on the UV/Ozone-pretreated surface. Correspondingly, the flake-like Ag NPs caused by jointed islands are observed on the H-terminated surface (Fig. 4b). The morphological difference of the Ag NPs suggests that the UV/Ozone-pretreated surface affects the nucleation of the in situ Ag NPs in the early stage of the MAEE process. As we know, the electroless deposition of Ag NPs belongs to an instantaneous nucleation mode (Yae et al. 2007). To observe the nucleation and the growth of Ag NPs on UV/Ozone-pretreated surface clearly, the concentrations of HF and $AgNO_3$ reduced to 0.25 and 0.001 M, respectively. Comparing with the H-terminated surfaces, the more uniform sizes of Ag NPs appear on the UV/Ozone-pretreated surfaces. In addition, particle density of Ag NPs is always higher on the UV/Ozone-pretreated surfaces than on the H-terminated surfaces during the deposition periods of 60 s, as described in Table 1. These results indicate that the UV/Ozone-pretreated surface improves the formation of the uniform and dense Ag NPs.

According to the above results, the roles of UV/Ozone pretreatment during the formation of SiNW arrays in $HF/AgNO_3$ solution are discussed. The nucleation behavior of Ag NPs is affected by the Si surface states. As we know, the Si wafers cleaned by a wet chemical-polished etching using CP-4A solution (Zhang 2001) have various surface defects, where the nucleation of Ag NPs occur preferentially. After HF processing, majority of surface defects are still present on the wafer and cause the nonuniform nucleation of Ag NPs (Fig. 5a). The UV/Ozone-pretreated process can produce a thin SiO_2 layer, which realizes the passivation to the surface defects. Nevertheless, the SiO_2 can stop the nucleation of Ag NPs because no electrochemical charge transfer between Si and the solution occurs. Therefore, the deposition of Ag NPs proceeds only on a bare Si surface accompanying the gradually chemical dissolution of thin SiO_2 layer by HF solution (Fig. 5d).

On the other hand, the growth process of Ag NPs is also affected by Si surface state. The growth of Ag NPs usually involves two possible ways. One way is the continuous reduction of Ag^+ ions on the Ag/Si interface. Another way is the assimilation among the adjacent Ag NPs. For the surface without thin SiO_2 layer, the growth of Ag NPs involves the above two

Fig. 3 **a** O 1s and **b** Si 2p photoelectron spectra of the Si surfaces treated by aqueous HF and UV/Ozone
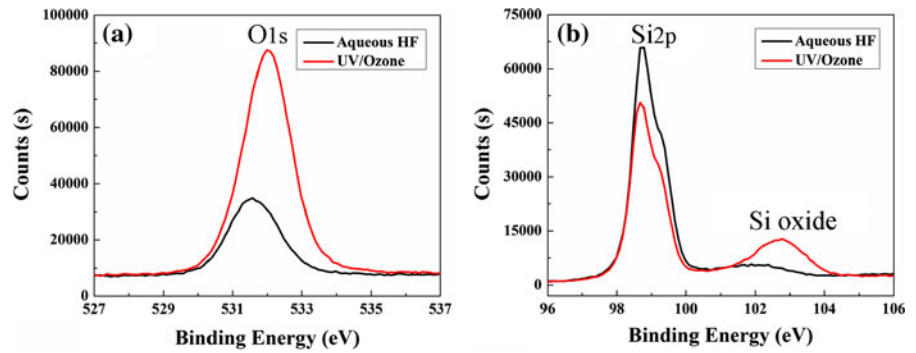

Fig. 4 SEM images of in situ Ag NPs on Si surfaces with **a** UV/Ozone pretreatment, and **b** H-terminated bonds
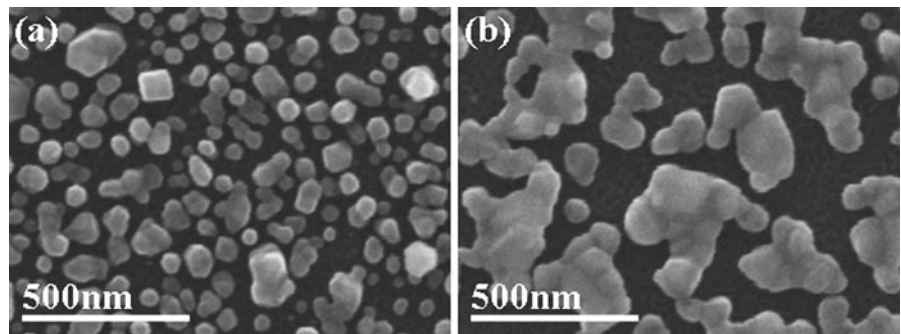

Table 1 Particle densities of Ag NPs on the H-terminated surfaces and the UV/Ozone-pretreated surfaces during different deposition times

Deposition time (s)	Particle density (cm^{-2})	
	UV/Ozone-pretreated surfaces	H-terminated surfaces
1	5.4×10^9	3.2×10^9
5	6.4×10^9	3.5×10^9
10	8.0×10^9	2.3×10^9
30	9.3×10^9	3.7×10^9
60	4.1×10^{10}	3.4×10^{10}

ways. It has been demonstrated that the smaller Ag NPs are usually assimilated into the larger Ag NPs through the electrons' transfer between NPs (Smith et al. 2013). Thus, the Ag NPs tend to form nonuniform flake-like structure (Fig. 5b), which results in the nonuniform coverage of SiNW arrays over the wafer (as shown in the left picture from Fig. 5c). For the surface with thin SiO_2 layer, the migration route of small Ag NPs toward large Ag NPs is obstructed owing to the presence of the retained SiO_2 layer between adjacent Ag NPs. Thus, the growth of Ag NPs is performed only according to the first way. Some Ag NPs grow on the initial nucleation sites, while the new

Ag nuclei also deposit among Ag NPs, both of which cause the deposition of uniform and dense Ag NPs (Fig. 5e). Finally, the uniform and dense Ag NP catalysts induce the formation of SiNW arrays with good uniformity and high filling ratio (Fig. 5f).

The uniform and dense SiNW arrays obtained by the UV-Ozone pretreatment process are of great importance for further practical applications. First, the antireflective property of the uniform and dense SiNW arrays is investigated. Compared with the original Si wafer, the SiNW arrays with a length of 0.7 μm sharply reduce the average reflectance from 38.6 to 4.4 % (Fig. 6a). As the length of SiNW arrays increases, the reflectance can be further reduced, especially for the longer wavelength ranging from 750 to 1,100 nm (insets in Fig. 6a). For the 5.7-μm-long SiNW arrays, the average reflectance is about 1.7 %, which approaches to the lowest values previously reported for 10-μm-long SiNW arrays (Ozdemir et al. 2011). The strong reduction of the surface reflection for the SiNW arrays is attributed to the high filling ratio caused by the process of UV/Ozone pretreatment.

Furthermore, the contact angles of water on the uniform and dense SiNW arrays are measured. As seen from Fig. 6b, the contact angle increases from 78° of original Si wafer to 123° of the uniform and dense
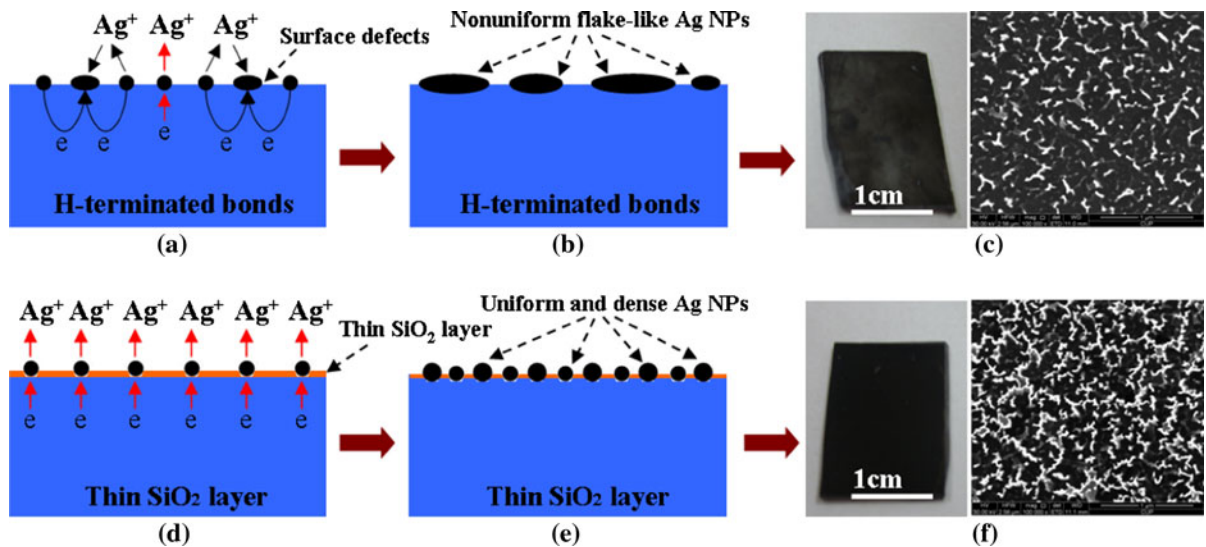
Fig. 5 Schematic diagrams of the formation of Ag NPs catalysts in HF/AgNO$_3$ solution on different surfaces: **a**, **b** are from H-terminated surface; **d**, **e** are from the surface with thin SiO$_2$ layer produced by UV/Ozone pretreatment; SEM Planar-viewed images and pictures of SiNW arrays on Si surfaces **c** with H-terminated bonds; and **f** with thin SiO$_2$ layer produced by UV/Ozone pretreatment, respectively

Fig. 6 a Average reflectance and **b** contact angles of water on the surface of SiNW arrays with *different lengths*; *Insets* in **a** show the reflection spectra of SiNW arrays with *different lengths*. *Insets* in **b** show the water droplets on the flat Si surface and the SiNW arrays, respectively
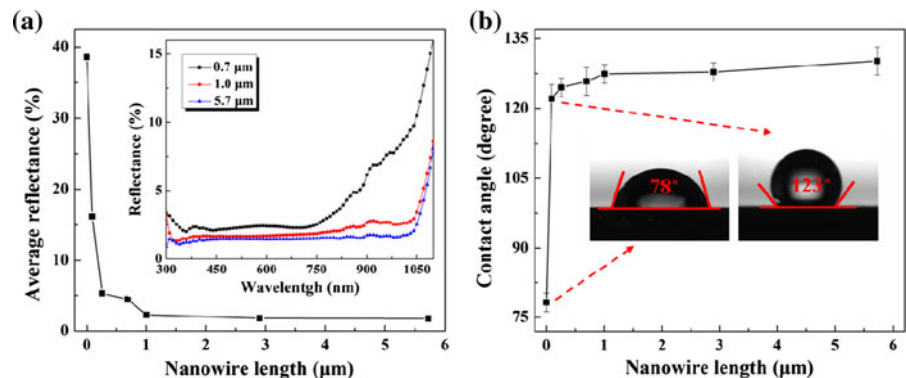
SiNW arrays prepared with the process of UV/Ozone pretreatment. With the increasing length of SiNW arrays, the contact angle is further increased up to 130°. The above results indicate that the uniform and dense SiNW arrays show remarkable antireflective and hydrophobic characteristics, which would create the opportunity of SiNW arrays for the applications in the wafer-scale self-cleaning antireflective layer.

Conclusion

In summary, we have reported a UV/Ozone pretreatment process to realize the wafer-scale fabrication of

SiNW arrays with good uniformity and high filling ratio in HF/AgNO$_3$ solution. The uniform 4-in. SiNW arrays are achieved. The almost similar SEM images at the random points of the sample, combining with the RSD value of reflection spectra below 0.2, reveal the wafer-scale uniformity of SiNW arrays. The Si surface with UV/Ozone pretreatment has a thin SiO$_2$ layer, which improves the deposition of uniform and dense Ag NPs catalysts, inducing the formation of SiNW arrays. Meanwhile, the SiNW arrays exhibit low average reflectance below 1.7 % in the wavelength range of 300–1,100 nm. Furthermore, these SiNW arrays can be employed as the hydrophobic surface, contact angle of which is as high as 130°. The proposed simple and cost-

effective fabrication technique for wafer-scale uniform SiNW arrays will enable the massive production of the wafer-scale self-cleaning antireflection layer.

References

Bai F, Li MC, Song DD, Yu H, Jiang B, Li YF (2012) One-step synthesis of lightly doped porous silicon nanowires in HF/AgNO$_3$/H$_2$O$_2$ solution at room temperature. J Solid State Chem 196:596–600

Chan CK, Peng H, Liu G, Mcilwrath K, Zhang XF, Huggins RA, Cui Y (2008) High-performance lithium battery anodes using silicon nanowires. Nat Nanotechnology 3(1):31–35

Dai YA, Chang HC, Lai KY, Lin CA, Chuang RJ, Lin GR, He JH (2010) Subwavelength Si nanowire arrays for self-cleaning antireflection coatings. J Mater Chem 20(48):10924–10930

Geng XW, Qi Z, Li MC, Duan BK, Zhu LJ (2012) Fabrication of antireflective layers on silicon using metal-assisted chemical etching with in situ deposition of silver nanoparticle catalysts. Sol Energy Mater Sol Cells 103:98–107

He Y, Jiang CY, Yin HX, Yuan WZ (2011) Tailoring the wettability of patterned silicon surfaces with dual-scale pillars: from hydrophilicity to superhydrophobicity. Appl Surf Sci 257(17):7689–7692

Jung JY, Um HD, Jee SW, Park KT, Bang JH, Lee JH (2013) Optimal design for antireflective Si nanowire solar cells. Sol Energy Mater Sol Cells 112:84–90

Krylyuk S, Davydov AV, Levin L (2011) Tapering control of Si nanowires grown from SiCl$_4$ at reduced pressure. ACS Nano 5(1):656–663

Mcalpine MC, Ahmad H, Wang DW, Heath JR (2007) Highly ordered nanowire arrays on plastic substrates for ultrasensitive flexible chemical sensors. Nat Materials 6(5):1–6

Morton KJ, Nieberg G, Bai SF, Chou SY (2008) Wafer-scale patterning of sub-40 nm diameter and high aspect ratio (>50:1) silicon pillar arrays by nanoimprint and etching. Nanotechnology 19(345301):1–6

Ozdemir B, Kulakci M, Turan R, Unalan HE (2011) Effect of electroless etching parameters on the growth and reflection properties of silicon nanowires. Nanotechnology 22(15):1–7

Peng KQ, Zhang ML, Lu AJ, Wong NB, Zhang RQ, Lee ST (2007) Ordered silicon nanowire arrays via nanosphere lithography and metal-induced etching. Appl Phys Lett 90(163123):1–3

Peng KQ, Wang X, Lee ST (2009) Gas sensing properties of single crystalline porous silicon nanowires. Appl Phys Lett 95(243122):1–3

Shiu SC, Lin SB, Hung SC, Lin CF (2011) Influence of pre-surface treatment on the morphology of silicon nanowires fabricated by metal-assisted etching. Appl Surf Sci 257(6):1829–1843

Smith ZR, Smith RL, Collins SD (2013) Mechanism of nanowire formation in metal assisted chemical etching. Electrochim Acta 92:139–147

Tamboli AT, Chen CT, Warren EL, Evans DBT, Kelzenberg MD, Lewis NS, Atwater HA (2012) Wafer-scale growth of silicon microwire arrays for photovoltaic and solar fuel generation. IEEE J Photovoltaics 2(3):294–297

Wang FY, Yang QD, Xu G, Lei NY, Tsang YK, Wong NB, Ho JC (2012a) Highly active and enhanced photocatalytic silicon nanowire arrays. Nanoscale 3(8):3269–3276

Wang W, Li D, Tian M, Lee YC, Yang R (2012b) Wafer-scale fabrication of silicon nanowire arrays with controllable dimensions. Appl Sur Sci 258(22):8649–8655

Yae SJ, Nasu N, Matsumoto K, Hagihara T, Fukumuro N, Matsuda H (2007) Nucleation behavior in electroless displacement deposition of metals on silicon from hydrofluoric acid solutions. Electrochim Acta 53(1):35–42

Zazzera LZ, Moulder JF (1989) XPS and SIMS study of anhydrous HF and UV/Ozone-modified silicon(100) surfaces. J Electrochem Soc 136(2):484–491

Zhang XG (2001) Electrochemistry of silicon and its oxide. Etching of silicon, 1st edn. Kluwer Academic/Plenum, New York, pp 293–294